Nano Energy 79 (2021) 105406

Contents lists available at ScienceDirect

Nano Energy

journal homepage: http://www.elsevier.com/locate/nanoen

Defect states contributed nanoscale contact electrification at ZnO nanowires packed film surfaces

Yiding Song [a,d], Nan Wang [a,d], Mohamed M. Fadlallah [b,f], Shuxia Tao [b,**], Ya Yang [a,d,e,*], Zhong Lin Wang [a,c,***]

[a] CAS Center for Excellence in Nanoscience, Beijing Key Laboratory of Micro-nano Energy and Sensor, Beijing Institute of Nanoenergy and Nanosystems, Chinese Academy of Sciences, Beijing, 100083, PR China
[b] Center for Computational Energy Research, Department of Applied Physics, Eindhoven University of Technology, P.O. Box 513, 5600MB, Eindhoven, the Netherlands
[c] School of Material Science and Engineering, Georgia Institute of Technology, Atlanta, GA, 30332-0245, USA
[d] School of Nanoscience and Technology, University of Chinese Academy of Sciences, Beijing, 100049, PR China
[e] Center on Nanoenergy Research, School of Physical Science and Technology, Guangxi University, Nanning, 530004, PR China
[f] Physics Department, Faculty of Science, Benha University, Benha, 13518, Egypt

ARTICLE INFO

Keywords:
Contact electrification
Direct current
Atomic force microscopy (AFM)
ZnO nanowires-packed film

ABSTRACT

Efficient conversion of mechanical energy in our surrounding environment into electric power has become a promising strategy for meeting the ever-increasing energy consumption of small and distributed electronics. The contact-electrification-based triboelectric nanogenerators are one of the emerging devices to achieve such energy conversion. However, conventional contact electrifications between two insulators are limited by their low current density and alternating current output. Here we report a nanoscale contact electrification induced direct current output based on the flow of electrons from the defect states of the ZnO nanowires-packed film to the contact sliding conductive AFM tip. Combining experimental materials characterization and density functional theory (DFT) calculations, the direct current output is closely related to the concentration of oxygen vacancy defect states on the surface of ZnO nanowires: the higher the oxygen vacancy concentration, the higher the current output. Under optimized conditions, we obtain an ultrahigh current density of $\sim 10^8$ A m^{-2}, which is several orders of magnitude higher than that of the conventional contact electrification and other effects. This work provides a new route of utilizing defect states contributed contact electrification for realizing nanoscale mechanical energy scavenging.

1. Introduction

The ever-increasing energy consumption has become one of the greatest challenges of the development of the modern society [1,2]. Scavenging mechanical energy from our surrounding environment [3–6] has attracted tremendous scientific efforts. The triboelectric nanogenerator (TENG) [7–12] is one of such promising devices to convert mechanical energy into electric power. Using TENG, various environmental mechanical energy sources such as human motion [7], rotating motion [8], vibration [9], water drop [10], sea wave [11], wind [12], etc., can be scavenged effectively. In conventional TENGs based on typical contact electrification, a pulsed AC output can be obtained by the periodical vertical/horizontal separation of two dielectric materials with opposite electrostatic charges. Although these devices generate a high output voltage, its output current density (J) is relatively low because of its high impedance. In order to obtain a DC output, some rectification methods, such as power management circuits [13] and rectifier bridge [14], are needed, resulting in poor portability and difficulties in the high-efficient utilization of energy. These characteristics block the widespread applications of these devices in wearable electronics and self-powered sensors, etc.

With the aim to convert mechanical energy directly into DC output,

* Corresponding author. CAS Center for Excellence in Nanoscience, Beijing Key Laboratory of Micro-nano Energy and Sensor, Beijing Institute of Nanoenergy and Nanosystems, Chinese Academy of Sciences, Beijing, 100083, PR China.
** Corresponding author.
*** Corresponding author. CAS Center for Excellence in Nanoscience, Beijing Key Laboratory of Micro-nano Energy and Sensor, Beijing Institute of Nanoenergy and Nanosystems, Chinese Academy of Sciences, Beijing, 100083, PR China.
E-mail addresses: s.x.tao@tue.nl (S. Tao), yayang@binn.cas.cn (Y. Yang), zhong.wang@mse.gatech.edu (Z.L. Wang).

https://doi.org/10.1016/j.nanoen.2020.105406
Received 19 August 2020; Received in revised form 9 September 2020; Accepted 17 September 2020
Available online 20 September 2020

dielectric breakdown has been used to realize a continuous DC output by sliding a metal electrode on the surface of polymer materials [15], which needs a large breakdown electric field of larger than 3 kV/mm, inducing a high impedance of these devices [16]. To obtain a DC output with low impedance, the metal electrodes have been utilized to directly slide on the surfaces of semiconducting materials [17–19]. The DC output has been found by sliding a metal tip on MoS_2 multi-layers due to that the electrons in MoS_2 may be excited from the valence band and the surface states to the conduction band, and then transmit into the metal side [17]. However, it is necessary to understand where the electrons come from: the valance band or the surface states. Moreover, if the electrons were excited into the conduction band, it is difficult to be unaffected by the built-in electric field in the depletion layer of Schottky junction, which will drive electrons to flow along the semiconductor side. By sliding a metal tip on the surface of n-type Si materials, an DC output can be observed due to the tribovoltaic effect, which is about the excitation of the electron and hole pairs in the conduction and valence band, respectively, by the energy released due to the formation of new bond at friction interface [18].

Inspired by the above progress, we used conductive atomic force microscopy (AFM) to demonstrate a DC output while sliding on a ZnO nanowires-packed film surface. Specifically, we propose defect states contributed nanoscale contact electrification between the conductive AFM tip and the ZnO nanowires-packed film, which is dominated for driving electrons to flow from defect states in ZnO nanowires to metal tip. The ZnO sample used here is literally a film that eliminates the transverse deflection of the nanowires composing the film during AFM scanning. This is different from the piezoelectric nanogenerator case of contact scanning AFM tip across spaced grown nanowires so that each nanowire can be deflected freely without any space restriction in the transverse directions [4,5]. Due to the tip-enhanced electrical field, the DC output exhibits an ultrahigh high current density in the order of 10^8 A m^{-2}, which is several orders of magnitude higher than that based on typical contact electrification and other effects. We systematically investigate the influence of various working conditions for the performances of the DC output and reveal the current response enhancement at surfaces of ZnO nanowires with higher concentrations of oxygen vacancy defect states, using larger contact force as well as slower scan rate. We also found that repeated scanning at the same location can attenuate the current output signal, but the attenuated signal can recover by itself with the recovery of oxygen vacancy density. This work provides an effective strategy of using the electrons in defect states of some nanomaterials to obtain DC output when the metal tip is sliding on the surfaces of these nanomaterials, offering a new method for nanoscale mechanical energy scavenging.

2. Experimental section

Synthesis. In a typical procedure, the ITO-coated glass substrates were cleaned ultrasonically with several times in glass clean agent, ethanol and deionized water, and then dried by high purity compressed air. Subsequently, a layer of ZnO seeds with thickness of about 150 nm was deposited on the cleaned ITO glasses by radio frequency (RF) magnetron sputtering (Ar atmosphere, room temperature) under a needed time and operating power. Then 2.9748 g zinc nitrate ($ZnNO_3{\cdot}6H_2O$) and 1.402 g hexamethylenetetramine (HMTA) were placed into deionized water (125 ml) under magnetic stirring to form a homogeneous growth solution. Meanwhile, seeded ITO substrates were fixed on a glass substrate and then immersed downward into the above growth solution, and the hydrothermal process was maintained at 85 °C for 4 h. Finally, the obtained ZnO nanowires-packed film was cleaned with deionized water, and then dried in a mechanical convection oven.

Characterization and Measurements. The prepared ZnO samples were observed by a field-emission scanning electron microscope (Nova NanoSEM 450). The photoluminescence (PL) spectra was obtained by fluorescence spectrometer (FLS980-S2S2-stm). The AFM measurements were achieved by using a commercial Tunneling Current AFM (PF-TUNA module)/KPFM equipment Dimension Icon (Bruker, USA) and Pt/Ir coated conductive-AFM probes (EFM, NanoWorld; force constant: 2.8 N/m; tip radius: 25 nm). It should be noted that, Tunneling Current AFM and Conductive Atomic Force Microscopy (C-AFM) have the same working principle and measurement method (both scan in Contact Mode), while Tunneling Current AFM has higher sensitivity and larger bandwidth (faster sampling rate). In the measurement process, simultaneous current and topographic images are generated by using the current amplifier and contact-mode scanning, respectively. Moreover, all AFM-based measurements were progressed in a glove box filled with dried nitrogen.

DFT calculations. All calculations on ZnO were achieved by utilizing density-functional theory (DFT) and the projector-augmented wave (PAW)/plane wave techniques, as implemented in the Vienna ab-initio simulation package (VASP) [20,21]. The geometry optimizations have been finished by using Perdew, Burke, and Ernzerhof (PBE) [22]. An energy cut-off of 500 eV and a k-point scheme of 6 × 6 × 1, and energy and force convergence parameters are set to 0.01 meV and 10 meV/Å, respectively. The calculated lattice constant of bulk wurtzite ZnO is 3.27 Å, which is consistent with the experimental value [23]. To calculate the formation energies of the oxygen vacancies and the work functions of the ZnO surfaces, (2 x 3) supercells of ZnO slabs, containing 6 repeating layers of Zn/O and a large vacuum of ~15 Å in z-direction were constructed. The work function (W_f) of the ZnO surfaces, using DFT, is calculated as follow:

$$W_f = E_0 - E_F \tag{1}$$

where E_0 and E_F are the vacuum potential and the Fermi energy of the surface, respectively. The dipole correction was considered in the calculations to enhance the electronic convergence [23] due to the polarity of (0001) and $(000\bar{1})$ surfaces. The formation energy of oxygen vacancy (Evac) is calculated as:

$$E_{vac} = E_{def} + \frac{N}{2}E(O_2) - E_{pri} \tag{2}$$

where E_{def}, N, $E(O_2)$, and E_{pri} are the DFT calculated total energies of the O-deficient surface, the number of O vacancy, the total energy of O_2 molecule and the total energy of the pristine surface, respectively.

3. Results and discussion

A schematic illustration of the DC generation has been exhibited in Fig. 1a, showing its basic configuration. The defect states contributed nanoscale contact electrification is demonstrated by sliding a Pt/Ir-coated silicon AFM tip on ZnO nanowires-packed film. When the AFM tip is rubbing on the ZnO sample, electrons can be transferred from the ZnO surface to the tip spontaneously and then flow to the ground through an external circuit, resulting in a negative DC signal. Fig. 1b depicts the cross-sectional scanning electron microscopy (SEM) image of the ZnO film. The ITO glass was covered by a layer of ZnO seeds with thickness of about 150 nm, then a layer of ZnO nanowires-packed film with a thickness of about 2 μm was grown on the ZnO seeds. The detailed synthesis process of the sample as given in the Experimental Section. The top-view SEM image of ZnO film (Fig. 1c), indicating high density and highly ordered hexagonal prism-shaped ZnO NWs on top of the ZnO seeds. As the tip scanned over the as-grown ZnO sample, the nanowires cannot be bent, because nanowires are very densely packed, just like a continuous film. Fig. 1d presents a typical AFM topographic mapping of the synthesized ZnO nanowires-packed film, where a quality topographic mapping can be obtained in contact mode, indicating that the nanowires maintain a good stability in the scanning process. The corresponding current mappings are displayed in Fig. 1e and f for trace and retrace channels, respectively. A DC signal can be observed from their cross-sectional line analysis (marked with white dashed line) and 3D

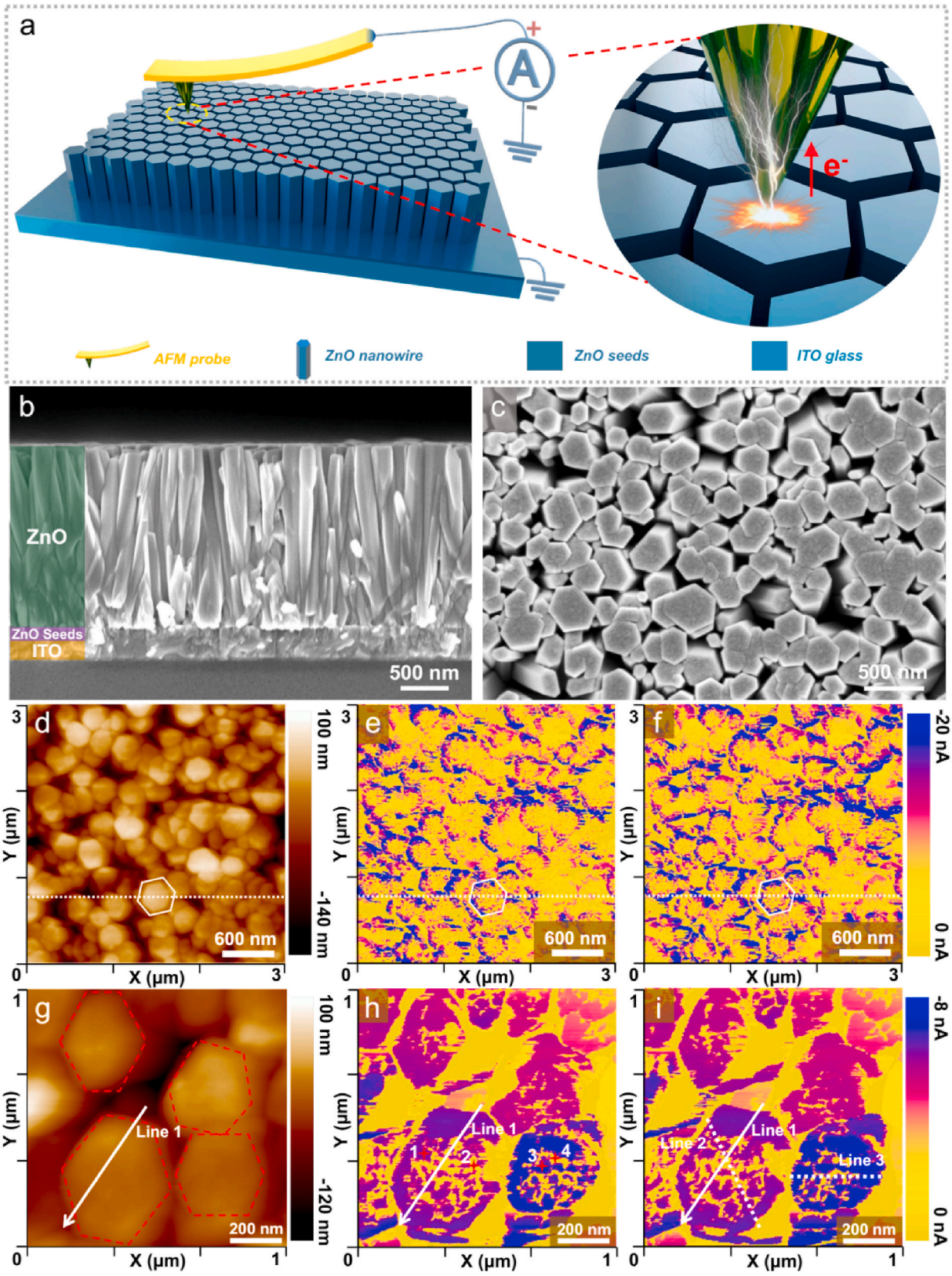

Fig. 1. The measurement method, material morphology and the corresponding output current mapping. (**a**) Schematic diagram of the measurement method. (**b,c**) SEM images of ZnO nanowires-packed film: cross-sectional view (b) and top view (c). (**d,e,f**) AFM topographic image of the ZnO nanowires-packed film at 3 μm scale (d) and the corresponding current mappings (e, f), (e) and (f) are trace and retrace channels respectively. A contact force of 232 nN was used here. (**g,h,i**) AFM topographic image of the ZnO sample at 1 μm scale (g) and the corresponding current mappings (h,i), (h) and (i) are trace and retrace channels respectively. A contact force of 160 nN was used here.

images of Fig. 1f (Fig. S1, Supporting Information). Meanwhile, the DC signal can be also obtained in AFM tapping mode (Fig. S2, Supporting Information), in which the AFM tip will compress ZnO nanowires vertically and then lift [4]. This is different from ZnO nanowires-based piezoelectric nanogenerators, which will produce an alternating piezoelectric signal with the application and release of the force [24,25]. It is worth noting that no external bias voltage is applied at any stages of the measurement. However, when there is external bias, the current signal can be enhanced with a negative sample bias and suppressed even reversed with a positive bias. The signal will be completely restrained when the bias reaches +5 mV (Fig. S3, Supporting Information), which is equivalent to the open-circuit voltage (V_{oc}) of the DC signal.

We note that almost no current is generated when the tip sliding on the layer of ZnO seeds or a ZnO film coated with tellurium (Figs. S4 and S5, Supporting Information), indicating that the DC output can only be generated by rubbing the surface of the as-grown ZnO nanowires. Such contact suggests that the DC output is highly sensitive to the morphology and the surface properties of the ZnO. The reproducibility of the DC output signal is very good as consistent overall pattern, and densities of the DC output are detected for different ZnO nanowires-packed films (Figs. S6 and S7, Supporting Information). Cross-sectional line analysis in Fig. 1h and i (marked with white arrow line: line 1) shows the current distribution on the single ZnO NW (Figs. S1c and S8, Supporting Information). Interestingly, the current signal generated at the edge of the nanowire is higher and more stable than that in the central region, which is associated with the distinct atomic surface structure of the top and side facets of the nanowires, as discussed later. The combination of the section analysis of the dashed line (line 2 and line 3 in Fig. 1i), and calculations using a simple Hertz model (Note S1, Supporting Information) allows us to determine an extremely high current density in the order of 10^8 A m^{-2}, which is several orders of magnitude higher than that based on typical contact electrification and other effects, as illustrated in Table S1 (Supporting Information). Such high current density may have to do with the drastically enhanced local electric field at the ZnO surface below the tip because of its point-plane contact configuration [17,26]. Fig. S8d (Supporting Information) illustrates the I-V curve marked with red dots in Fig. 1h and their equivalent circuits. It can be found in the I-V data that a Schottky contact is formed across the metal-semiconductor interface. Moreover, no apparent difference in the I-V curves is found at the different positions, indicating that the Schottky barrier heights across the top surfaces are almost identical and the work function of the AFM tip (Pt/Ir) is higher than that of the ZnO ($W_m > W_s$).

We then illustrate the working mechanisms in Fig. 2a and Fig. S9 (Supporting Information). The mechanism of the DC output is based on the defect states contributed nanoscale contact electrification, meanwhile, the contact electrification process is dominated by electron transfer, which is consistent with previous research [27,28]. To understand the mechanism of the DC output, we used density functional theory (DFT) to calculate the work functions of the Pt metal tip and the ZnO semiconductor surfaces. Subsequently, we construct energy band diagrams in Fig. 2e and f, where the friction process between the nano-sized tip and a point on the ZnO surface is demonstrated. For the work function of ZnO, we considered pristine and O-deficient (0001), $(000\bar{1})$, and $(10\bar{1}0)$ surfaces (Fig. 2b), the most commonly reported surfaces for ZnO nanowires [29]. We find an average work function of 4.4 eV, where $(10\bar{1}0)$ is the lowest (3.3 eV) and (0001) and $(000\bar{1})$ are much higher (5.3 eV and 5.5 eV), respectively. The work function of $(000\bar{1})$ surface (Zn-termination) is higher than that of (0001) surface (O-termination) due to the metallicity of $(000\bar{1})$. The work function of the Pt (111) surface (the AFM tip) is calculated to be 5.9 eV, higher than all those of ZnO surfaces. The values reported in this work for both ZnO and Pt are consistent with previous theoretical reports [30–33]. Also, it is important to be noted that as-prepared ZnO nanowires are known to have high densities of surface oxygen vacancies as native defects. Previous DFT calculations show that oxygen vacancies create defect states at the mid-gap which can trap the excited electrons [34].

Altogether, the work function of the AFM tip (Pt/Ir) is higher than that of the ZnO (semiconductor) ($W_m > W_s$) (Fig. 2e). When the tip has a contact with a point on ZnO surface of the nanowire, a Schottky junction across the metal-semiconductor interface is formed. It should be noted that the electrons will obey the Fermi-Dirac function in this surface states model, as follows:

$$f = \frac{1}{exp^{(E-E_F)/kT} + 1} \tag{3}$$

where f is the probability of an electron in the energy level of E, E_F denotes the Fermi level, k is the Boltzmann constant, and T is the temperature [35,36]. As displayed in Equation (3), at the temperature of T, the electrons can be excited, where the corresponding increased electron energy (ΔE) is approximately kT, due to that the experiment is performed at room temperature higher than 0 K. Before the metal tip has a contact with ZnO surface, the electrons in the ZnO surface states will be not excited into the vacuum level, because the increased electron energy (ΔE) is not large enough. As shown in Fig. 2e, Fermi level of the metal tip (Pt/Ir) is higher than the ZnO and there are electrons in the surface states below the Fermi level of ZnO [37,38]. When the metal tip has an effective contact with ZnO surface, the Fermi levels of metal and semiconductor will be aligned, which results in band bending and upward shifting of surface states on semiconductor side [38]. Therefore, the surface states previously below the Fermi level of ZnO are now higher than the aligned Fermi levels. The electrons previously trapped by oxygen vacancy will be excited and transferred from the ZnO nanowires to the metal tip because the highest occupied surface state level of the ZnO is higher than the Fermi level of metal, as exhibited in Fig. 2f. During the sliding process, the electrons at the metal side would meet a high Schottky barrier, so it is hard for them to get back to the semiconductor side, the electrons in the ZnO surface states will be constantly released due to the driving of ΔE and transported to the ground through the external circuit, and then realizing the DC signal. When the probe slides forward, it will contact the next point on the ZnO surface, a new Schottky junction will be established and the surface state and the band at the interface shift up together again, and then the electrons at the surface states above Fermi level of ZnO will flow into the metal. Thus, during sliding the electrons will be continuously transfer to the AFM tip. In addition, electrons from surface states will not excited to the conduction band. If electrons are excited to the conduction band, according to the tribovoltaic effect [18,39,40], electrons will transfer from metal to semiconductor driven by built-in electric field, which is contrary to the observed current signal.

To elaborate on the underlying reasons for the different current densities on the edge and centers of the ZnO nanowires in Fig. 1h and i, we focus on the influence of the O vacancy concentrations. We find the work function of ZnO only slightly decreases (about 0.1–0.2 eV) as the concentration of the O vacancy increases from 0 to 3.75% in Fig. 2c. While this small work function shift does not change the overall band alignment we established above, oxygen defects do introduce mid-gap states. Because O-deficient ZnO is an n-type semiconductor [41,42] and the Fermi energy is close to the conduction band [34] more surface charge carriers can be created for n-type ZnO as compared to the pristine ZnO. After the alignment of the Fermi energy of metal and n-type ZnO in Fig. 2f, and at a close distance between the tip and the n-type ZnO nanowires, the electrons can be transferred from n-type ZnO to metal tip and further flow to the external circuit.

The above analysis indicates that the current generated is originated from trap states associated with the oxygen vacancy defects and the current density relates strongly with the concentration of the oxygen vacancies. Our DFT calculations (Fig. 2d) show that the oxygen vacancy formation energies increase drastically from $(10\bar{1}0)$ to (0001) and to $(000\bar{1})$ with formation energies of 0.46, 1.27 and 3.42 eV/atom, respectively. This indicates that the as-fabricated ZnO nanowires exhibit

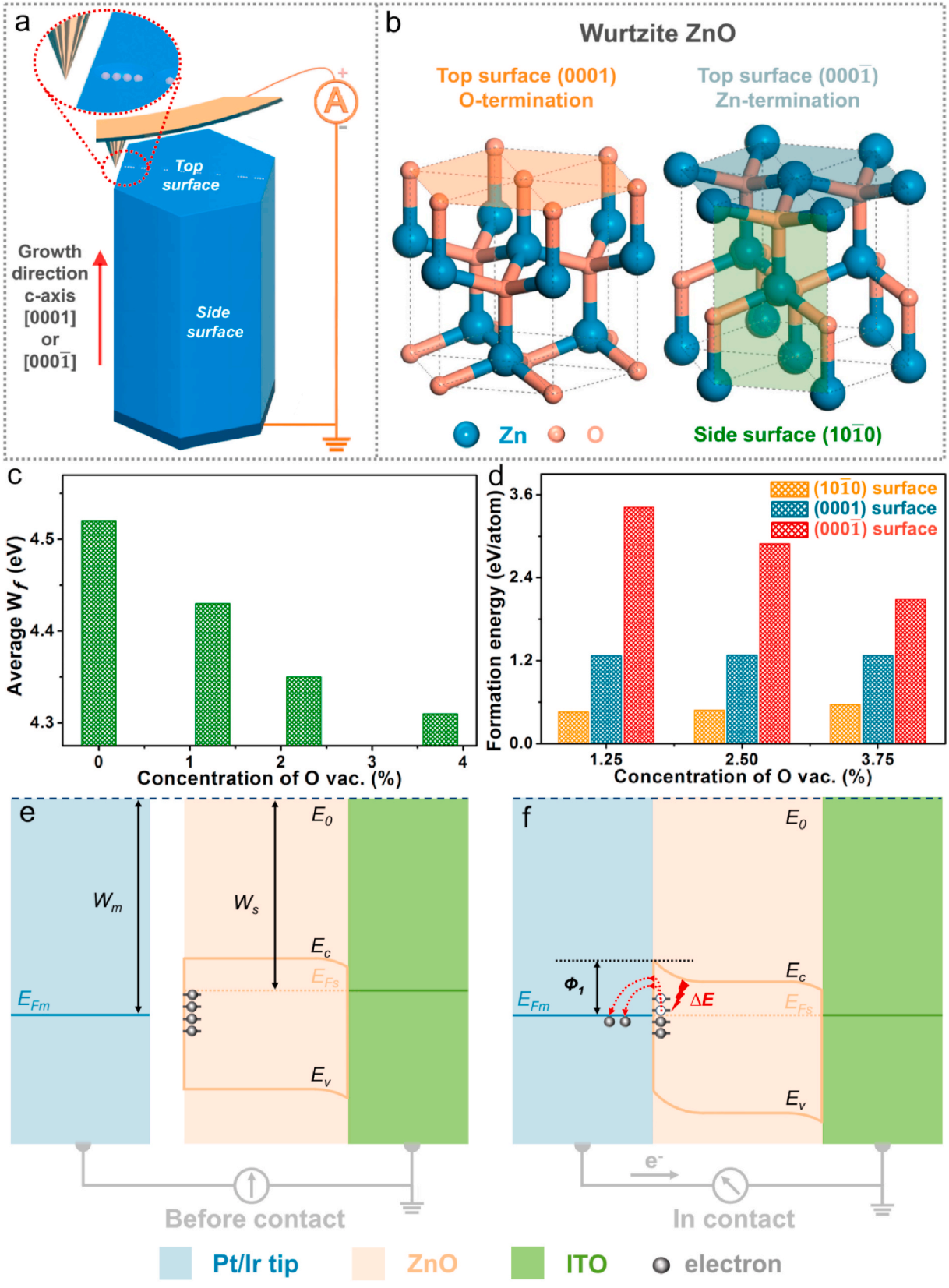

Fig. 2. Mechanisms of the DC output. (**a**) The mechanisms of the DC output based on defect states contributed nanoscale contact electrification. (**b**) The DFT optimized ZnO surfaces: (0001) surfaces, (000$\bar{1}$) surfaces (sub-layered oxygen vacancy) and (10$\bar{1}$0) surfaces, respectively. (**c,d**) the average work function of the three surfaces shown in (b) and the oxygen vacancy formation energy (normalized to per oxygen vacancy) as a function of the concentration of O vacancies (d). (**e,f**) Energy band diagram of the working process: before contact (e), in contact electrification (f).

an intrinsic inhomogeneous distribution of the oxygen vacancies: the side $(10\bar{1}0)$ surface potentially has much higher number of oxygen vacancies than the top (0001) and $(000\bar{1})$ surfaces. This is consistent with our experimental observation, where the larger and more stable current can be found on the edge than that on the center of the nanowires.

After having established the working principles, the influence of working conditions on the DC output has been investigated, including the scan rate and the contact force. Fig. 3a displays a topographic AFM image of the ZnO sample with different four scan rates. As illustrated in Fig. 3b, c and d, a higher DC signal response and higher current density can be obtained at a slower scan rate. More detailed results and analysis are given in Fig. S10 (Supporting Information). The derived average

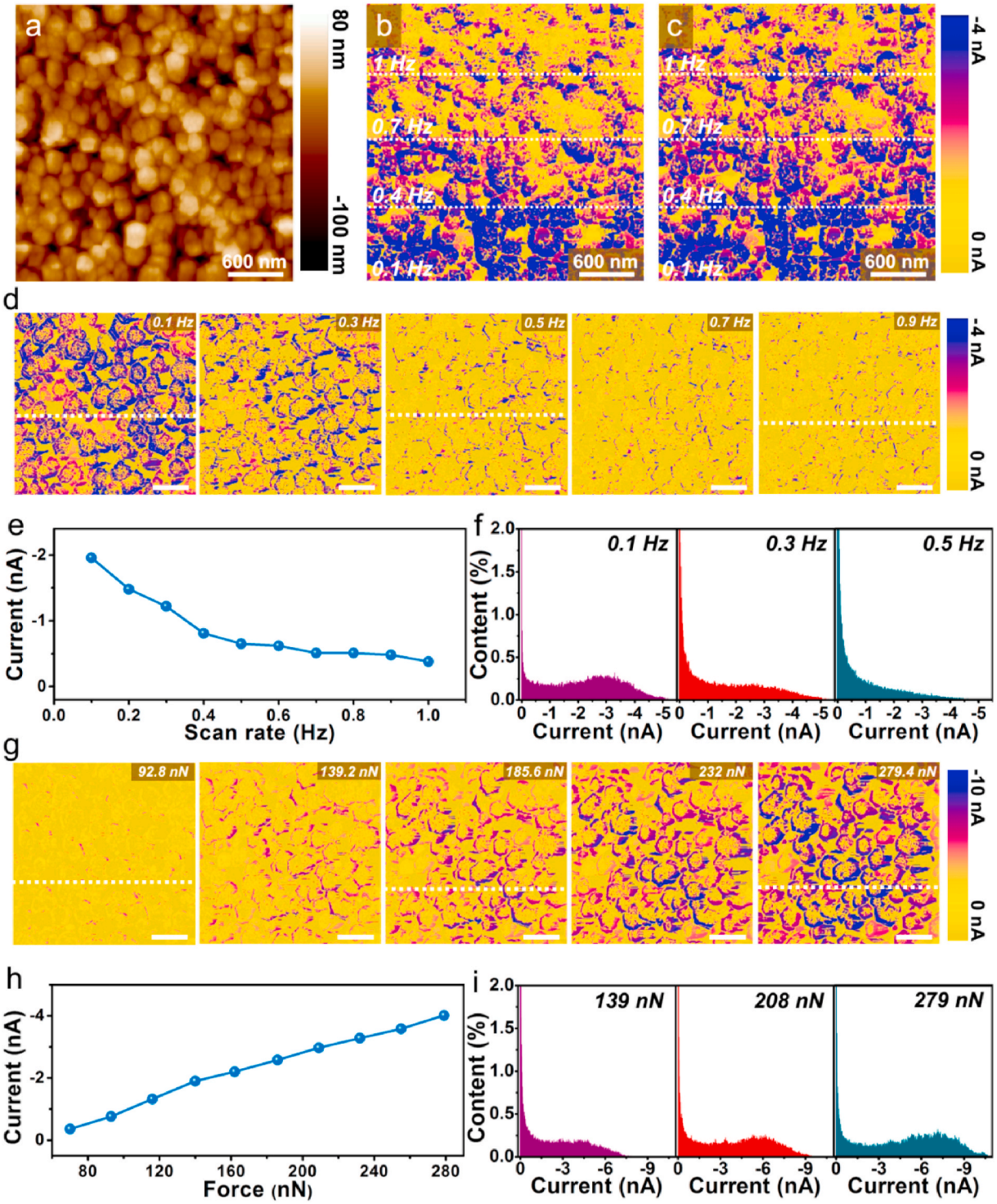

Fig. 3. The scan rate and contact force dependent measurements. (**a,b,c**) AFM topographic image of the ZnO sample (a) and the corresponding current mappings at different scan rates (b,c), (b) and (c) are trace and retrace channels respectively. (**d,e,f**) Scan rate dependent current signal with increasing scan rate (d), corresponding relationship between average current of current mappings and the increasing scan rate (e) and statistics of the current signal using different scan rates (f). (**g,h,i**) Force dependent current signal; current mappings with the contact force changes from small to large (g), corresponding average current of current mappings (h) and statistics of the current signal using different contact forces (i). Scale bars, 600 nm (d), 600 nm (g).

current I_{ave} decreases from 1.96 nA to 0.38 nA when the scan rate increases from 0.1 Hz to 1 Hz, as depicted in Fig. 3e. By comparing the statistics in Fig. 3f, the proportion of larger current signal decreases with increasing the scanning rate. However, when a position is rubbed repeatedly, the current signal will decay, which is associated with Joule heating, as discussed latter. We investigate the current response when the scan rate changes from fast to slow further. It can be observed that a higher current signal can still be obtained at a slower scanning rate although there was the influence of current attenuation (Fig. S11, Supporting Information). The slower sliding rate of the probe on ZnO can

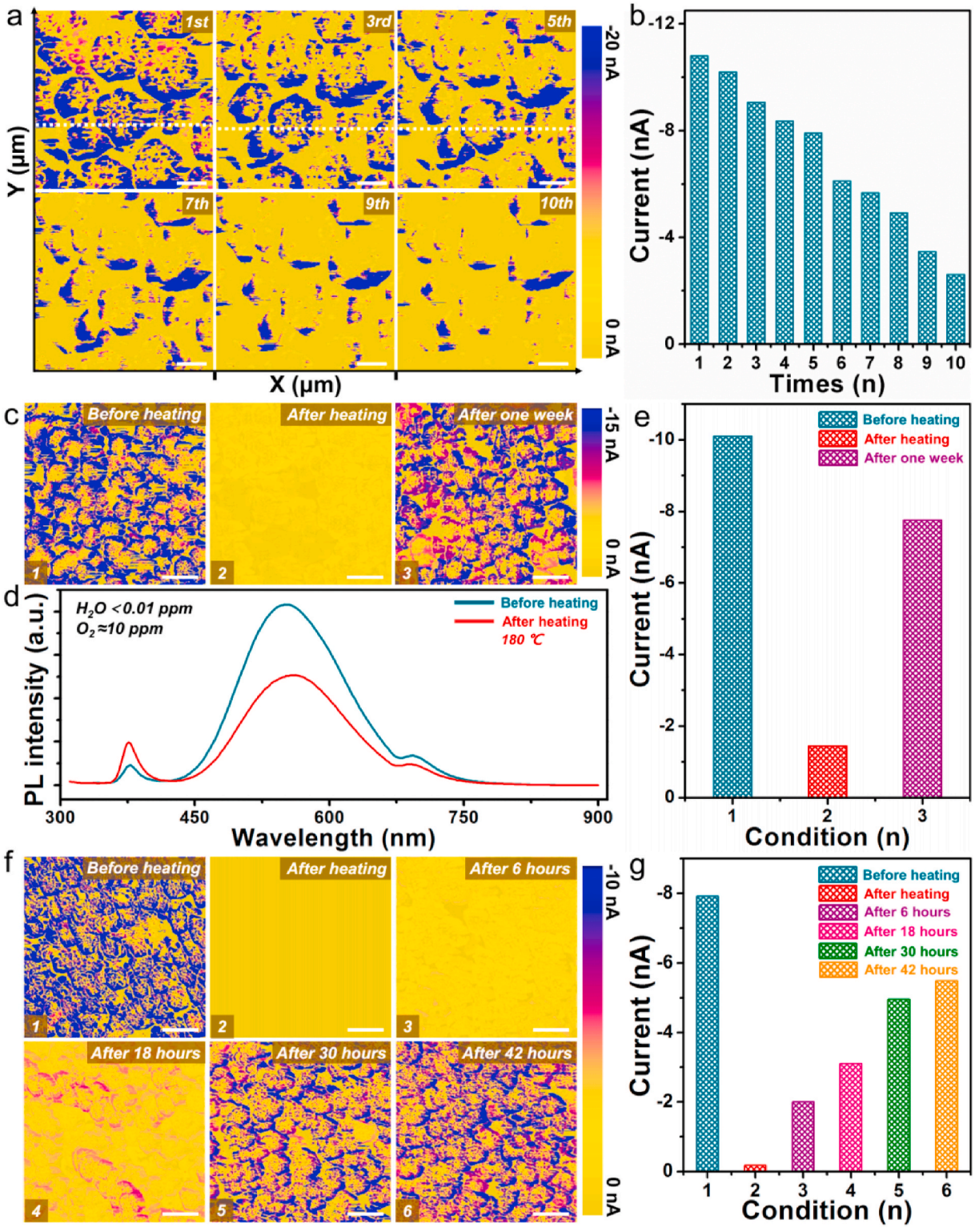

Fig. 4. The stability of the DC output. (**a**) Current mappings with different repeated times of scanning. (**b**) The decay of average current induced by repeated scanning. (**c,d,e**) Current mappings of ZnO sample under different conditions (c), corresponding PL spectra of the ZnO sample before and after heating (d) and average current under different conditions (e). (**f,g**) Current mappings of the ZnO sample before heating, after heating, after 6 h, after 18 h, after 30 h and after 42 h (f), and corresponding average current in different conditions (g). Scale bars, 200 nm (a), 600 nm (c), 600 nm (f).

result in the larger current signal, which is associated with the frictional heat caused by the mechanical friction during the scanning. It can enhance electron scattering between metal-semiconductor interfaces, then affecting the electron transfer process. When the probe slides on the sample, a retarding force (kinetic friction force F) will be imposed on the probe, and such friction force generates the mechanical friction heat. Here, when the probe slides a distance x, the work W_F done by the kinetic friction force can be regarded as:

$$|W_F| = \int_0^x F dx \tag{4}$$

Unlike macro-scale, the friction force is related to the velocity v of the friction at the nanoscale. This velocity-dependent friction can be theoretically interpreted by Prandtl-Tomlinson (PT) model and a stick-slip behavior at the nanoscale [43–45]. Previous AFM investigations have reported a logarithmic increase in nanoscale friction with velocity, the relationship between the nanoscale stick-slip-related friction force and the velocity can be described as:

$$f(v) = a_1 + a_2 ln \frac{v}{v_1} \tag{5}$$

where a_1 and a_2 are characteristic coefficients and v_1 is a critical sliding velocity, when the friction velocity is greater than v_1, the logarithmic growth will slow down [44,45]. Therefore, the W_F can be modified as:

$$|W_F| = \int_0^x \left(a_1 + a_2 ln \frac{v}{v_1}\right) dx \tag{6}$$

The above expression indicates that the slower the scanning rate can induce the less heat generated, so that the easier the electrons will be transferred to the tip, therefore resulting in a larger current signal. This is different from the tribovoltaic effect, in which the faster the friction speed will excite more electrons transition to the conduction band and achieving higher current output [18].

Moreover, the influence of the contact force on the current output has been investigated. The current distribution versus applied force (F) is displayed in Fig. 3g. An increased current response can be observed with increased F. More detailed results and analysis are given in Fig. S12 (Supporting Information). Here, the effect of current attenuation caused by repeated friction has been excluded, because of the sequence of the forces applied in the experiments (F changes from small to large). As illustrated in Fig. 3h, the average current I_{ave} increases with increasing the contact force. Moreover, by using larger contact force, the probability of finding higher current signal also increases, as presented in Fig. 3i. According to the Hertz model discussed in Note S1 (Supporting Information), upon increasing the force, the tip-sample contact area increases. The larger contact area makes better electrical contact, which is beneficial to electron transfer, thus, allows enhanced current distribution and therefore increased I_{ave}.

We finally investigate the stability of the current output. As depicted in Fig. 4a and b, repeated scanning at the same position will attenuate the average current and current mapping signal distribution. Detailed results and analysis are exhibited in Fig. S13 (Supporting Information). After scanning the same position twice and then shift the friction position slightly, the current response in the new position (without friction by the probe) was found to be much higher. This indicates that the reduction of the current signal is unlikely due to the tip damage but very likely because of the variations of the surface characteristics of the ZnO caused by friction (Fig. S14, Supporting Information).

Because of the point-contact geometry at the nanoscale of the AFM system (tip-plane), a small voltage between tip and sample can lead to a drastically enhanced local electrical field [17,26]. Due to the tip-enhanced electrical field, an ultrahigh current density can occur, resulting in that the large Joule heating can also be generated [46]. As mentioned earlier, when the number of O vacancies increases the output current increases. The Joule heating generated during the DC power generation could reduce the density of the O vacancies on ZnO surface. This hypothesis is consistent with the analysis in the next paragraph, where smaller concentration of oxygen vacancy can be found at the surfaces of ZnO upon heating at 180 °C as compared with that at room temperature from PL and XPS analysis. As a result, the current signal is attenuated after repeated friction. As compared with the reduction trend of the edge and the center area, it can be found that the signal decay of the edge part is much slower. From the current mapping with a fixed line place (AFM probe is only scanning in the x-direction, no scanning of the sample in the y-direction is performed, as illustrated in Fig. S15, Supporting Information), the current signal at the center area decays rapidly, while the current signal at some of the edges remains similar. It is associated with the higher oxygen vacancy concentration on the edges of the nanowires, so that the edges will be less affected by the oxygen vacancy attenuation caused by Joule heat during friction.

Moreover, we also investigated the variations for the work function of the ZnO surface before and after the friction using the Kelvin probe force microscopy (KPFM). Using KPFM, the work function difference between the sample and tip (i.e. $W_{Potential} = W_{sample} - W_{probe}$) can be determined. As depicted in Fig. S16 (Supporting Information), the surface potential of the rubbed region is 0.11 V higher than that of the unrubbed region. The slightly increasing surface work function here is due to the reduction of oxygen vacancies [47], which is also consistent with our DFT predictions in Fig. 2c. Based on the above analysis, oxygen vacancy defect states play a key role in our DC generation. As we mentioned above, the tip-enhanced electrical field could generate large Joule heating between the tip and sample, which has been applied and confirmed in the research of nanopatterning and electric-induced nano-damage using conductive AFM tip [48–50]. Here, the Joule heating induced by both the DC generation and friction of AFM tip may reduce the density of the oxygen vacancy on the top surfaces of ZnO nanowires so that fewer electrons trapped by oxygen vacancy, lead to less electrons transfer in the contact electrification process, and therefore the current attenuates, which is consistent with the mechanism of the DC output. To understand the effect of heating further, the entire sample is heated at 180 °C in the glove box filled with nitrogen to simulate the situation when the sample is heated by the tip. As illustrated in Fig. 4c, the current signal is obviously attenuated after heating. At the same time, the attenuation of the current response can still be observed by rubbing the same position repeatedly on the heated sample, which can be attributed to the fact that the probe continues to heat the sample (Fig. S17, Supporting Information).

To understand the influence of the change for the surface stoichiometry on the generated current, we carry out the photoluminescence (PL) analysis to investigate the density of surface defect states of ZnO. As displayed in Fig. 4d, the PL spectra of the ZnO sample before and after heating exhibits three peaks centered at 378 nm, about 550 nm, about 694 nm. It is generally confirmed that the peak at 378 nm is associated with the recombination of electrons in the conduction band and the holes in the valence band; the broad peak at about 550 nm is associated with surface defects such as oxygen vacancies, whereas the emission peak at about 694 nm has been found to explain the presence of excess oxygen on the ZnO surface [47,51–53]. It can be observed that the peak at 550 nm decreases significantly after heating, which is associated with the heating induced reduction of the surface traps such as surface oxygen vacancies. Heating stimulates the migration of the intrinsic defects in the ZnO nanowires. For example, interstitial zinc (Zn_i), known to be very mobile owing to their low migration barrier of 0.57 eV [54], may migrate to and occupy the site of oxygen vacancy and forms the zinc anti-site (Zn_O), reducing the number of the oxygen vacancies [55]. The formation energy of the zinc anti-site, however, thermodynamically unstable, as evidenced by its high formation energy [56]. As a result, the number of oxygen vacancy recovers gradually with time, which is consistent with the recovery of attenuated current signal. Further X-ray photoelectron spectroscopy (XPS) experiments corroborate the analysis

above, as depicted in Fig. S18 (Supporting Information). The O 1s XPS spectra for ZnO can be fitted with three Gaussian peaks located at 530.2 (O_{III}), 531.25 (O_{II}), and 532.1 (O_I) eV, which can be attributed to O^{2-} ions in the Zn-O bonding in the ZnO lattice, oxygen vacancy, and chemisorbed oxygen such as -OH, adsorbed H_2O, O_2, etc., respectively (Fig. S18c, Supporting Information). As compared with the sample before heating, the relative spectral area of the oxygen vacancy decreases from 32.21% to 24.58% after heating, clearly indicating that the density of oxygen vacancy is reduced upon heating.

It can be noted that we find a similar recovery phenomenon in samples after heating (in Fig. 4c and e) and the repeated scanning in Fig. S19 (Supporting Information). As illustrated in Fig. 4e, the average current decreases from 10.1 nA to 1.44 nA upon heating at 180 °C while it can recover to 7.75 nA after a week later. As displayed in Fig. S20e (Supporting Information), both the DC signal and the attenuated PL oxygen vacancy defect-related peak can recover after one week, confirming that the current signal can be restored once the oxygen vacancy density is restored. The same phenomenon has been observed in heating experiments at 90 °C (Fig. S21, Supporting Information). To explore the possible effect of water, a heated sample is first placed in an atmosphere with a humidity of 60% for 2 h in order to absorb some water on its surface and then stored in the glove box, and the DC output response of the sample can be measured at regular intervals (Fig. S22, Supporting Information). For comparison, a heated ZnO sample is kept in the glove box filled with dry nitrogen after heating, then its attenuated current signal recovers gradually with time (Fig. 4f, g and Fig. S23, Supporting Information). The current signal recovers neither faster nor slower via the absorption of water, suggesting that the effect of water can be excluded.

4. Conclusion

In summary, the DC output of nanoscale contact electrification between an AFM tip and ZnO nanowires-packed film has been investigated. Due to the tip-enhanced electrical field at nanoscale, the obtained DC output exhibits an ultrahigh high current density of 10^8 A m^{-2}, which is much higher than those of previous strategies based on typical contact electrification and other effects. Our combined experimental (XPS, PL and KPFM) and theoretical (DFT calculations) analysis reveals that the performance of the DC output is closely associated with the density of the oxygen vacancies defect states on the ZnO surfaces. The current density decays with decreasing the number of the oxygen vacancies, which is associated with the Joule heating during repeated frictions of the probe and the surfaces of the ZnO nanowire. Notably, the attenuated DC output signal can be recovered by itself upon cooling with the recovery of oxygen vacancy density. Moreover, it has been found that both large contact force and slow scan rate can enhance the current output because the former improves the contact area and the latter reduces the heat of mechanical friction. Our work provides a potential strategy for obtaining DC output from nanoscale contact electrification without any rectification methods. We believe this nano-scale effect can be improved further through the optimization of the friction materials as well as the overall device configurations, offering a new method for using nanoscale contact electrification to drive the electrons in the defect states of some materials, realizing nanoscale mechanical energy scavenging.

CRediT author statement

Yiding Song: contributed equally, fabricated the materials and carried out the performance measurement, Formal analysis, analyzed the data and co-wrote the manuscript. All authors contributed to the final version of the manuscript. **Nan Wang:** contributed equally, fabricated the materials and carried out the performance measurement. **Mohamed M. Fadlallah:** contributed equally, performed DFT calculations, Formal analysis, analyzed the data and co-wrote the manuscript. All authors contributed to the final version of the manuscript. **Shuxia Tao:** Supervision, DFT work, Formal analysis, analyzed the data and co-wrote the manuscript. All authors contributed to the final version of the manuscript. **Ya Yang:** Supervision, conceived the idea and supervised the research, Formal analysis, analyzed the data and co-wrote the manuscript. All authors contributed to the final version of the manuscript. **Zhong Lin Wang:** Supervision, conceived the idea and supervised the research, Formal analysis, analyzed the data and co-wrote the manuscript. All authors contributed to the final version of the manuscript.

Declaration of competing interest

The authors declare that they have no known competing financial interests or personal relationships that could have appeared to influence the work reported in this paper.

Acknowledgments

Y.S., N.W. and M.F. contributed equally. This work was supported by the National Key R&D Program of China (Grant No. 2016YFA0202701), the National Natural Science Foundation of China (Grant No. 51472055), External Cooperation Program of BIC, Chinese Academy of Sciences (Grant No. 121411KYS820150028), the 2015 Annual Beijing Talents Fund (Grant No. 20150000021223ZK32), Qingdao National Laboratory for Marine Science and Technology (No. 2017ASKJ01), and the University of Chinese Academy of Sciences (Grant No. Y8540XX2D2). S.T. acknowledges funding by the Computational Sciences for Energy Research (CSER) tenure track program of Shell and NWO (Project Number 15CST04-2), the Netherlands.

Appendix A. Supplementary data

Supplementary data to this article can be found online at https://doi.org/10.1016/j.nanoen.2020.105406.

References

[1] Z.L. Wang, Faraday Discuss 176 (2014) 447–458.
[2] Z.L. Wang, J. Chen, L. Lin, Energy Environ. Sci. 8 (2015) 2250–2282.
[3] X. Wang, J. Song, J. Liu, Z.L. Wang, Science 316 (2007) 102–105.
[4] Z.L. Wang, J. Song, Science 312 (2006) 242–246.
[5] J. Song, J. Zhou, Z.L. Wang, Nano Lett. 6 (2006) 1656–1662.
[6] J. Nie, X. Chen, Z.L. Wang, Adv. Funct. Mater. 29 (2019) 1806351.
[7] K. Zhang, X. Wang, Y. Yang, Z.L. Wang, ACS Nano 9 (2015) 3521–3529.
[8] H. Yang, Y. Pang, T. Bu, W. Liu, J. Luo, D. Jiang, C. Zhang, Z.L. Wang, Nat. Commun. 10 (2019) 2309.
[9] J. Chen, Z.L. Wang, Joule 1 (2017) 480–521.
[10] Q. Zhang, Q. Liang, Q. Liao, M. Ma, F. Gao, X. Zhao, Y. Song, L. Song, X. Xun, Y. Zhang, Adv. Funct. Mater. 28 (2018) 1803117.
[11] J. Chen, J. Yang, Z. Li, X. Fan, Y. Zi, Q. Jing, H. Guo, Z. Wen, K.C. Pradel, S. Niu, Z. L. Wang, ACS Nano 9 (2015) 3324–3331.
[12] B. Chen, Y. Yang, Z.L. Wang, Adv. Energy Mater. 8 (2018) 1702649.
[13] X. Wang, Y. Yang, Nano Energy 32 (2017) 36–41.
[14] C. Zhang, T. Zhou, W. Tang, C. Han, L. Zhang, Z.L. Wang, Adv. Energy Mater. 4 (2014) 1301798.
[15] D. Liu, X. Yin, H. Guo, L. Zhou, X. Li, C. Zhang, J. Wang, Z.L. Wang, Sci. Adv. 5 (2019), eaav6437.
[16] Y. Yang, H. Zhang, Z.L. Wang, Adv. Funct. Mater. 24 (2014) 3745–3750.
[17] J. Liu, A. Goswami, K. Jiang, F. Khan, S. Kim, R. McGee, Z. Li, Z. Hu, J. Lee, T. Thundat, Nat. Nanotechnol. 13 (2018) 112–116.
[18] Z. Zhang, D. Jiang, J. Zhao, G. Liu, T. Bu, C. Zhang, Z.L. Wang, Adv. Energy Mater. 10 (2020) 1903713.
[19] S. Lin, Y. Lu, S. Feng, Z. Hao, Y. Yan, Adv. Mater. 31 (2019) 1804398.
[20] G. Kresse, J. Furthmuller, Comput. Mater. Sci. 6 (1996) 15–50.
[21] G. Kresse, J. Furthmuller, Phys. Rev. B 54 (1996) 11169–11186.
[22] J.P. Perdew, K. Burke, M. Ernzerhof, Phys. Rev. Lett. 77 (1996) 3865–3868.
[23] S. Desgreniers, Phys. Rev. B 58 (1998) 14102.
[24] S. Lu, Q. Liao, J. Qi, S. Liu, Y. Liu, Q. Liang, G. Zhang, Y. Zhang, Nano Res. 9 (2016) 372–379.
[25] S.N. Cha, J.-S. Seo, S.M. Kim, H.J. Kim, Y.J. Park, S.-W. Kim, J.M. Kim, Adv. Mater. 22 (2010) 4726–4730.
[26] M. Alexe, D. Hesse, Nat. Commun. 2 (2011) 256.
[27] C. Xu, A.C. Wang, H. Zou, B. Zhang, C. Zhang, Y. Zi, L. Pan, P. Wang, P. Feng, Z. Lin, Z.L. Wang, Adv. Mater. 30 (2018) 1803968.

[28] A.C. Wang, B. Zhang, C. Xu, H. Zou, Z. Lin, Z.L. Wang, Adv. Funct. Mater. 30 (2020) 1909384.
[29] K.M. Wong, S.M. Alay-e-Abbas, Y. Fang, A. Shaukat, Y. Lei, J. Appl. Phys. 114 (2013), 034901.
[30] R.M. Hewlett, M.A. McLachlan, Adv. Mater. 28 (2016), 3893-3821.
[31] F.-L. Kuo, Y. Li, M. Solomon, J. Du, N.D. Shepherd, J. Phys. D Appl. Phys. 45 (2012), 065301.
[32] W. Sun, Y. Li, J.K. Jha, N.D. Shepherd, J. Du, J. Appl. Phys. 117 (2015) 165304.
[33] A. Patra, J.E. Bates, J. Sun, J.P. Perdew, Proc. Natl. Acad. Sci. Unit. States Am. 114 (2017) E9188–E9196.
[34] F. Oba, M. Choi, A. Togo, I. Tanaka, Sci. Technol. Adv. Mater. 12 (2011), 034302.
[35] Z.L. Wang, A.C. Wang, Mater. Today 30 (2019) 34–51.
[36] S. Lin, L. Xu, C. Xu, X. Chen, A.C. Wang, B. Zhang, P. Lin, Y. Yang, H. Zhao, Z. L. Wang, Adv. Mater. 31 (2019) 1808197.
[37] H. Zou, G. Dai, A.C. Wang, X. Li, S.L. Zhang, W. Ding, L. Zhang, Y. Zhang, Z. L. Wang, Adv. Mater. 32 (2020) 1907249.
[38] H. Zou, L. Guo, H. Xue, Y. Zhang, X. Shen, X. Liu, P. Wang, X. He, G. Dai, P. Jiang, H. Zheng, B. Zhang, C. Xu, Z.L. Wang, Nat. Commun. 11 (2020) 2093.
[39] M. Zheng, S. Lin, L. Xu, L. Zhu, Z.L. Wang, Adv. Mater. 32 (2020) 2000928.
[40] S. Lin, X. Chen, Z.L. Wang, Nano Energy 76 (2020) 105070.
[41] B.J. Jin, S.H. Bae, S.Y. Lee, S. Im, Mater. Sci. Eng. B 71 (2000) 301–305.
[42] C.H. Patterson, Phys. Rev. B 74 (2006) 14432.
[43] E. Gnecco, R. Bennewitz, T. Gyalog, C. Loppacher, M. Bammerlin, E. Meyer, H. J. Guntherodt, Phys. Rev. Lett. 84 (2000) 1172–1175.
[44] E. Riedo, E. Gnecco, R. Bennewitz, E. Meyer, H. Brune, Phys. Rev. Lett. 91 (2003), 084502.
[45] N.S. Tambe, B. Bhushan, Nanotechnology 16 (2005) 2309–2324.
[46] Y. Yang, J. Qi, Y. Gu, W. Guo, Y. Zhang, Appl. Phys. Lett. 96 (2010) 123103.
[47] D. Kim, K.Y. Lee, M.K. Gupta, S. Majumder, S.-W. Kim, Adv. Funct. Mater. 24 (2014) 6949–6955.
[48] J. Song, M.A. Hempenius, H.J. Chung, G.J. Vancso, Nanoscale 7 (2015) 9970–9974.
[49] D. Mashiyama, T. Tobe, T. Ogino, J. Phys. Chem. C 119 (2015) 11914–11921.
[50] P. Huang, D. Guo, G. Xie, J. Li, Nano Lett. 17 (2017) 6280–6286.
[51] S. Bai, Y. Jin, X. Liang, Z. Ye, Z. Wu, B. Sun, Z. Ma, Z. Tang, J. Wang, U. Wuerfel, F. Gao, F. Zhang, Adv. Energy Mater. 5 (2015) 1401606.
[52] B. Panigrahy, M. Aslam, D.S. Misra, M. Ghosh, D. Bahadur, Adv. Funct. Mater. 20 (2010) 1161–1165.
[53] J.J. Schneider, R.C. Hoffmann, J. Engstler, O. Soffke, W. Jaegermann, A. Issanin, A. Klyszcz, Adv. Mater. 20 (2008) 3383–3387.
[54] A. Janotti, C.G. Van de Walle, Phys. Rev. B 76 (2007) 165202.
[55] E.G. Barbagiovanni, R. Reitano, G. Franzo, V. Strano, A. Terrasi, S. Mirabella, Nanoscale 8 (2016) 995–1006.
[56] A.F. Kohan, G. Ceder, D. Morgan, C.G. Van de Walle, Phys. Rev. B 61 (2000) 15019–15027.

Yiding Song is currently a master degree candidate in the research group of Prof. Ya Yang at Beijing Institute of Nanoenergy and Nanosystems, Chinese Academy of Sciences (CAS). His recent research interests are new energy harvesting strategy and atomic force microscopy.

Nan Wang is a postdoc in the research group of Prof. Ya Yang at Beijing Institute of Nanoenergy and Nanosystems, Chinese Academy of Sciences (CAS). She received her Ph.D. in electroanalytical chemistry, from Changchun Institute of Applied Chemistry, CAS. Her research interests focus on direct-current triboelectric nanogenerator and mechanical properties of 2D materials.

Dr. Mohamed M. Fadlallah received his Ph.D. in Physics from the Institute of Physics, Augsburg University, Augsburg, Germany in 2010. Currently, he is an associate professor in the Faculty of Science, Physics Department, Benha University, Benha, Egypt. He was a visiting researcher and post-doctor at Augsburg University, Augsburg, Germany, and Center for Computational Energy Research, Department of Applied Physics, Eindhoven University of Technology, Eindhoven, the Netherlands. His area of expertise is computational materials science with a focus on the electronic, transport, and photocatalytic properties of metal oxides, one-, two-, and three-dimensional structures.

Dr. Shuxia Tao received her PhD of Computational Materials Science from Eindhoven University of Technology (TU/e), the Netherlands. After three years as post-doctoral researcher at NIKHEF, she currently is an Assistant Professor at TU/e. With two prestigious personal grants, CSER tenure track and NWO START-UP, she currently leads a young research group Computational Materials Physics. Her research interests lie in the development and application of Density Functional Theory and multiscale computational methods in the area of novel energy conversion and storage technologies. More details of her research can be found at: https://www.shuxiatao.com/.

Prof. Ya Yang received his Ph.D. in Materials Science and Engineering from University of Science and Technology Beijing, China. He is currently a professor at Beijing Institute of Nanoenergy and Nanosystems, Chinese Academy of Sciences, China. He has developed various new hybridized and multi-effects coupled devices, opening up the new principles of the device design and coupled effects, and the new approaches of improving output performances of energy-related devices. His main research interests focus on the field of hybridized and coupled devices for energy conversion, self-powered sensing, and some new physical effects. Details can be found at: http://www.researcherid.com/rid/A-7219-2016.

Prof. Zhong Lin (ZL) Wang received his Ph.D. from Arizona State University in physics. He now is the Hightower Chair in Materials Science and Engineering, Regents' Professor, Engineering Distinguished Professor and Director, Center for Nanostructure Characterization, at Georgia Tech. Dr. Wang has made original and innovative contributions to the synthesis, discovery, characterization and understanding of fundamental physical properties of oxide nanobelts and nanowires, as well as applications of nanowires in energy sciences, electronics, optoelectronics and biological science. His discovery and breakthroughs in developing nanogenerators established the principle and technological road map for harvesting mechanical energy from environment and biological systems for powering personal electronics. His research on self-powered nanosystems has inspired the worldwide effort in academia and industry for studying energy for micro-nano-systems, which is now a distinct disciplinary in energy research and future sensor networks. He coined and pioneered the field of piezotronics and piezophototronics by introducing piezoelectric potential gated charge transport process in fabricating new electronic and optoelectronic devices. Details can be found at: http://www.nanoscience.gatech.edu.